Low-frequency guided waves in a fluid-filled borehole
Simultaneous effects of generation and scattering due to multiple fractures

Minato, Shohei; Ghose, Ranajit

DOI
10.1063/1.4978250

Publication date
2017

Document Version
Accepted author manuscript

Published in
Journal of Applied Physics

Postprint of Journal of Applied Physics
Volume 121, 104902 (2017)
Link to formal publication : http://dx.doi.org/10.1063/1.4978250

Low-frequency guided waves in a fluid-filled borehole: simultaneous effects of generation and scattering due to multiple fractures

Shohei Minato[1, a)] and Ranajit Ghose[1, b)]

Department of Geoscience and Engineering, Delft University of Technology, 2628 CN Delft, the Netherlands

(Dated: 10 February 2017)

Low-frequency, axially-symmetric guided waves which propagate along a fluid-filled borehole (tube waves) are studied in order to characterize the hydraulic fractures intersecting the borehole. We formulate a new equation for the total tube wavefield, which includes simultaneous effects of (1) tube-wave scattering (reflection and transmission) due to wave propagation across hydraulic fractures, and (2) tube-wave generation due to incident plane P waves. The fracture is represented by the nonwelded interface boundary conditions. We use an appropriate form of the representation theorem in order to correctly handle the multiple scattering due to nonwelded interfaces. Our approach can implement any model that has so far been developed. We consider a recent model which includes simultaneous effects of fluid viscosity, dynamic fluid flow, and fracture compliance. The derived equation offers a number of important insights. We recognize that the effective generation amplitude contains the simultaneous effect of both tube-wave generation and scattering. This leads to a new physical understanding indicating that the tube waves are scattered immediately after generation. We show that this scattering is nonlinear with respect to interface compliance. This physical mechanism can be implicitly accounted for by considering more realistic boundary conditions. We also illustrate the application of the new equation in order to predict the complex signature of the total tube wavefield including generation and scattering at multiple hydraulic fractures. A new formulation for focusing analyses is also derived in order to image and characterize the hydraulic fractures. The obtained results and discussions are important for interpretation, modeling and imaging using low-frequency guided waves, in the presence of multiple fractures along a cylindrical inclusion.

PACS numbers: 46.40.-f,46.50.+a,91.30.-f,43.20.+g

Keywords: Surface waves, Waveguides, Tube waves, Acoustic wave scattering, Rock fracture, Wave attenuation, Cracks

[a)]Electronic mail: s.minato-1@tudelft.nl

[b)]Electronic mail: r.ghose@tudelft.nl

I. INTRODUCTION

Guided waves are widely studied in the context of estimating mechanical and hydraulic properties of materials. The utility of guided waves is well-established in nondestructive material testing, e.g., for composite laminates[1–3] and cylindrical shells immersed in a fluid.[4,5] There is a growing interest in medical sciences where guided waves at long bones are investigated in order to diagnose osteoporosis or to evaluate the healing of a fracture bone.[6,7] In applied seismology, the guided waves are extensively used for predicting wave propagation along a fluid-filled borehole.[8,9]

The dispersion of the velocity of guided waves is often utilized to characterize material properties. Another important wave phenomenon, which is observed in different fields, is the scattering (reflection and transmission) of guided waves due to material heterogeneities, e.g., defects, cracks and fractures. Scattered guided waves are of direct relevance in, e.g., inspection of pipes,[10] examining composite laminates,[3] monitoring the condition of mechanical structures,[11] and characterizing hydraulic fractures in a borehole.[12]

The axially-symmetric guided waves along a cylindrical circular inclusion have been extensively studied in the past.[8,13] Their low-frequency parts, traveling along a fluid-filled cylindrical hole embedded in an elastic medium, are what we call in this study the low-frequency Stoneley waves or the tube waves.[8,14]

In both exploration and earthquake seismology, characterizing the hydraulic fractures is important because hydraulic fractures play a key role in controlling the fluid flow in the subsurface.[15,16] In this vein, tube waves are useful in formation characterization in the vicinity of a borehole.[17] They are powerful in providing information on permeability corresponding to μm-to-mm scale fractures,[12,18] as well as larger-scale (cm-to-m) geological faults.[19,20]

Similar to applications in nondestructive material testing, scattering of tube waves at hydraulic fractures have also been utilized to estimate the fracture properties.[12,18,21–23] The mechanism of tube-wave scattering is generally formulated in terms of the fluid exchange between the fracture and the borehole, due to the perturbation in fluid pressure at the intersection. The problem of a parallel-wall open fracture was first considered by Mathieu [21] and later extended by Refs. 12, 22, and 23. Furthermore, the propagation of tube wave across a poroelastic layer, instead of a parallel-wall fracture, was considered in Refs. 22 and

24.

In addition to tube-wave scattering, the generation of tube waves at hydraulic fractures due to an external source located at the Earth's surface is well known.[25] This is explained by fluid exchange between the borehole and the fracture due to the deformation of the fracture. Beydoun *et al.*[25] first presented the theoretical formulations regarding the amplitude of the generated tube waves in terms of fracture properties (e.g., fracture aperture and static permeability), assuming a parallel-wall open fracture and the Darcy's law. Ionov[26] further studied the effect of the dynamic permeability model.[24] The tube-wave generation due to the deformation of a poroelastic layer, instead of a parallel wall fracture, can be found in Ref. 19. The recent studies of elastic wave propagation across a fracture reveal that the fracture compliance (dynamic fracture closure due to the applied stress) is a key to infer the fracture properties, such as, roughness of the fracture surface, contact asperities, and fracture infill materials.[27–30] In this vein, the effect of the fracture compliance in the generated tube waves was investigated in several past studies.[18,23,31]

Although the generation and the scattering of tube waves have been independently studied, their simultaneous effects have not yet been looked at. In field measurements, the tube-wave generation amplitudes are evaluated by extracting (windowing) recorded tube waves at downhole receivers, and compare with the incident pressure in order to estimate the tube to P-wave amplitude ratio.[18–20,23,25,31] The tube-wave scattering is evaluated by extracting first the tube waves and then estimating the reflection/transmission coefficients.[12,18,21–23] This involves the assumption of a single fracture or sparsely-spaced fractures, and the simultaneous effects of generation and scattering and those of multiple fractures are not considered. The accurate prediction of the complex signatures of total tube wavefield and the analysis of the closely-spaced multiple fractures are especially important in a highly fractured area, such as a fault-damaged zone, whose permeability structure controls the deformation processes within the crust.[16]

The goal of this study is to represent the total tube wavefield including the simultaneous effects of reflection, transmission and generation due to multiple hydraulic fractures. A key component in deriving the equation is the representation of hydraulic fractures as nonwelded interfaces across which the particle velocity is discontinuous but the acoustic pressure is continuous. The problem becomes that of an one-dimensional multiple scattering of scalar waves due to multiple, simultaneously acting sources whose excitation times are shifted by

the arrival time of the incident wave.

A conventional approach to predict multiple scattering in one-dimensional media contains the integral equation of the scattering potential function.[32] In the case of acoustic or elastic media, the potential functions have been conventionally related to the impedance contrast, e.g., perturbation of elastic constants and densities from background.[33–35] In addition to the effect of the contrasting medium parameters, however, we need to introduce the nonwelded interfaces in order to correctly handle the multiple scattering due to hydraulic fractures. To this end, we use the recent forms of the representation theorem[36] which includes the effect of nonwelded interface in general wave equation, and we derive the representation theorem of the tube wavefield. We then utilize the existing theories of tube-wave generation and tube-wave scattering to represent the total tube wavefield.

Some recent studies clarify the explicit connections between the representation theorem and the Green's function retrieval which is considered as a powerful tool in Acoustics and Seismics.[37–39] Therefore, deriving the total tube wavefield using the representation theorem gives an implicit connection to this research. For this purpose, the representation theorem is exploited in order to address the elastic scattering problem in case of multiple fractures and a method to image the fractures.[40]

As mentioned above, there are a variety of models that account for the generation and scattering of tube waves. However, owing to its great flexibility, the use of an appropriate representation theorem enables one to implement any model that has so far been developed. Although we study here the interaction of tube waves (guided waves in a fluid-filled borehole) with multiple fractures, the concept has a broad implication, as it can be useful in nondestructive material testing and medical sciences, where detecting and characterizing small defects/cracks/fractures along a cylindrical inclusion (e.g., pipes, bones) is often of importance.

We first present the theory that is necessary to derive the total tube wavefield. We next show the application of the developed theory to a single fracture, and identify that the simultaneous effects of tube-wave generation and scattering lead to a new physical interpretation of the effective tube-wave generation amplitude. We also illustrate the application of the equation for total tube wavefield to imaging and characterizing multiple hydraulic fractures using the total tube wavefield. We finally present numerical modeling examples to validate the theory developed in this study.

II. THEORY

Throughout the paper, we define the temporal Fourier transform as

$$f(\omega) = \int_{-\infty}^{\infty} f(t) \exp(i\omega t) dt, \tag{1}$$

where $i^2 = -1$ and ω is the angular frequency.

Considering quasi-static wave propagation (i.e., low-frequency approximation) along the fluid-filled borehole, the one-dimensional acoustic wave equation is derived.[22,41] We formulate the constitutive relation and the equation of motion which are represented using vertical particle velocity $v_z(z)$ and acoustic pressure $p(z)$ of the borehole fluid:

$$-i\omega K_{\text{eff}}^{-1} p + \frac{\partial v_z}{\partial z} = q, \tag{2}$$

$$-i\omega \rho_f v_z + \frac{\partial p}{\partial z} = f_z, \tag{3}$$

where ρ_f is the density of the borehole fluid, q is the injection-rate source, and f_z is the external vertical-force source. K_{eff} is the effective bulk modulus of the borehole fluid and is a function of the fluid bulk modulus (K_f), the shear modulus of the formation (μ), and the wall impedance (Z_R) due to fluid flow through the permeable solid:[41,42]

$$K_{\text{eff}}^{-1} = K_f^{-1} + \mu^{-1} - 2(i\omega R Z_R)^{-1}, \tag{4}$$

where R is the borehole radius. The solutions of Eqs. (2) and (3) with impulsive sources (i.e., Green's functions) are characterized by the tube-wave velocity c_T:

$$c_T^{-2} = \rho_f K_{\text{eff}}^{-1}. \tag{5}$$

We consider two physical mechanisms for the interaction of the tube waves with the hydraulic fractures intersecting the borehole: (1) the generation of tube waves and (2) the scattering (reflection and transmission) of tube waves. We formulate the equation for the total tube wavefield by simultaneously considering these two mechanisms using a representation theorem. As we have discussed in the previous section, there is a large variety of models that account for these two mechanisms. In this paper, we focus on the open-fracture model which is recently developed by Bakku *et al.*,[23] because it includes almost all the features that other foregoing studies separately investigated (i.e., the effects of fluid viscosity, dynamic permeability, and facture compliance).

In this section, we first briefly review the existing model of tube-wave generation amplitude ratio. Secondly, we show the scattering (reflection and transmission) model and the relation with nonwelded interface representation of the fracture. We then present the representation theorem including nonwelded interfaces for the tube wavefield. Finally, we derive a new equation for total tube wavefield, including reflection, transmission and generation due to multiple hydraulic fractures.

A. Tube-wave generation amplitude ratio

Tube waves are generated at hydraulic fractures and are modeled as a fluid pulse injected into a borehole due to compression and dilatation of the fracture (Fig. 1a). Here, we consider that the fracture has horizontal, parallel walls with constant (small) aperture L_0, and a normally-incident plane P-wave causes the oscillation of the fracture wall.[23,25,26,31] We consider the model developed by Bakku *et al.*[23] which is briefly discussed in Appendix A 1, as this is necessary to derive the amplitude using boundary conditions which are suitable for investigating the simultaneous effects of the generation and scattering (Appendix A 2). The key component in deriving the generation amplitude is the fluid flux in the fracture per unit length q_f (m^2/s). Bakku *et al.*[23] assumed that q_f satisfies the dynamic fluid flow condition for a rigid fracture,[24] and they incorporated the effect of the fracture compliance through a perturbation in the dynamic aperture (L, see Eq. A1) and the mass-conservation equation (see Appendix A 1 for detail).

The pressure distribution in the fracture $p_F(r,\omega)$, where r is the radial distance, is solved from the mass-conservation equation (Eq. A2) using appropriate boundary conditions. As we show in Appendix A 1, two different sets of boundary conditions are proposed: Beydoun's boundary condition (Appendix A 2) and Bakku's boundary condition (see Appendix A 1). Beydoun *et al.*[25] considered that the pressure perturbation at the fracture-borehole intersection $p_F(R,\omega)$ is negligibly small. On the other hand, Bakku *et al.*[23] considered a more realistic boundary condition in which the pressure at the borehole intersection is equivalent to the generated tube-wave amplitude.

As we will show later in Section III, we consider the simultaneous effects of tube-wave generation and scattering using the representation theorem. This gives us a new physical interpretation for the effective tube-wave generation amplitudes, i.e., scattering immediately

after generation. In order to correctly account for this physical mechanism, we require an adequate boundary condition in deriving the tube-wave generation amplitude (p_t). To this end, we revisited the boundary conditions first considered in Beydoun *et al.*[25] in order to solve the mass-conservation equation proposed by Bakku *et al.*[23].

Beydoun *et al.*[25] considered the following boundary conditions:

$$\left.\frac{\partial p_F(r,\omega)}{\partial r}\right|_{r=\infty} = 0, \tag{6}$$

$$p_F(r,\omega)|_{r=R} = 0. \tag{7}$$

The first equation (Eq. 6) states that the pressure is bounded at infinity and the second equation (Eq. 7) indicates that the fluid pulse injected into the borehole does not perturb the borehole pressure.[25] In this case, the generated tube wave (p_t) is derived as (see Appendix A 2),

$$p_t(\omega) = \sigma_0 \frac{i\omega c_T}{k_r \alpha_f} \frac{\rho_f Z \alpha_{\text{eff}}}{R} \frac{H_1(\zeta R)}{H_0(\zeta R)}, \tag{8}$$

where Z is the fracture compliance (m/Pa), ζ and α_{eff} are, respectively, the effective radial wavenumber and the effective fluid velocity in the fracture (Eq. A3), σ_0 is the amplitude of the normally-incident plane P wave, and $H_n = H_n^{(1)}$ is a Hankel function of the first kind and order n. Here, k_r is the radial wavenumber in the rigid fracture obtained by numerically solving the dispersion relation developed in Ref. 24, and k_r is a function of the kinematic fluid viscosity (ν), fluid velocity (α_f), static fracture aperture (L_0), and angular frequency (ω). For completeness, the generated amplitude derived from Bakku's original boundary conditions (Eqs. A5 and A6) is shown in Eq. (A10). Note that when there is no incident wave ($\sigma_0 = 0$) or when one considers a rigid fracture ($Z = 0$), tube waves are not generated ($p_t = 0$, see Eq. 8) because the acoustic wave is not excited in the fracture (see Eq. A2). Furthermore, when one considers a rigid fracture ($Z = 0$), then the problem reduces to the wave propagation in the fluid layer with constant thickness[12] and we obtain $\alpha_{\text{eff}} = \alpha_f$ (Eq. A3). The fracture compliance (Z) can be frequency dependent due to the heterogeneity along the fracture surface and/or the effect of fluid flow.[43–45] Using the quasi-static approximation for a thin, parallel-wall fracture filled with fluid,[46] the fracture compliance may be represented as $Z \approx L_0/K_f$.

Eq. (8) indicates that the generated tube waves depend on the amplitude of the P wave (σ_0). Therefore, we derive the tube to P-wave amplitude ratio γ_g to remove the effect of σ_0

(Refs. 18, 19, 23, 25, 26, and 31). The incident pressure field in the borehole ($p_{\rm inc}$) due to normally-incident plane P wave with amplitude σ_0 is written as,[41]

$$p_{\rm inc}(\omega) = \sigma_0 \frac{\rho_f c_T^2}{\rho V_S^2} \left(\frac{1 - 2V_S^2/V_P^2}{1 - c_T^2/V_P^2} \right), \tag{9}$$

where ρ, V_P and V_S are density, P-wave velocity and S-wave velocity in the formation, respectively. Evaluating the amplitude ratio (γ_g) of the incident P wave and the generated tube wave eliminates σ_0:

$$\gamma_g = \frac{p_t}{p_{\rm inc}}. \tag{10}$$

B. Tube-wave scattering and nonwelded interface representation of a fracture

When tube waves intersect a hydraulic fracture, a part of the fluid flows into the fracture, which creates reflected and transmitted waves (Fig. 1b). The problem of a parallel-wall open fracture with constant (small) aperture L_0 was first considered by Mathieu [21] and later extended by Refs. 12 and 23. The common assumption in these studies is that the fluid volume flux across the fracture in the borehole is conserved as follows:

$$\pi R^2 \left[v_z(-L_0/2) - v_z(+L_0/2) \right] - 2\pi R \, q_f|_{r=R} = 0, \tag{11}$$

where the fracture is assumed to be located at $z = 0$, and $q_f|_{r=R}$ is the fluid flux which flows from the borehole to the fracture at the borehole wall. Eq. (11) states that the difference in the fluid flux in the borehole across the fracture is equivalent to the fluid flow into the fracture. Tang and Cheng [22] pointed out that Eq. (11) can be derived by applying the divergence theorem of Gauss to the equation of continuity and ignoring the dynamic volume compression at the borehole, and they revealed that this condition is adequate as long as the aperture L_0 is small.

The fluid flux q_f is obtained differently in different studies.[12,21–23] Among them, Bakku *et al.*[23] derived q_f considering the simultaneous effects of fluid viscosity, dynamic fluid flow, and fracture compliance (see Appendix A 1 and A 3 for detail). From Eqs. (A4) and (A16), the fluid flux can be written as,

$$q_f|_{r=R} = p\zeta \frac{i\omega L_0}{k_r^2 \alpha_f^2 \rho_f} \frac{H_1(\zeta R)}{H_0(\zeta R)}, \tag{12}$$

where p is the fluid pressure in the borehole.

From Eqs (11) and (12), we obtain the following boundary condition at the fracture:

$$\Delta v_z = i\omega\eta p, \tag{13}$$

$$\eta = -\frac{2\zeta}{R}\frac{L_0}{k_r^2\alpha_f^2\rho_f}\frac{H_1(\zeta R)}{H_0(\zeta R)}, \tag{14}$$

where Δv_z is a discontinuity in vertical particle velocity across the fracture, i.e., $\Delta v_z = v_z(+L_0/2) - v_z(-L_0/2)$, and interface compliance η linearly relates the velocity discontinuity to the acoustic pressure. Here we further assume that the pressure is continuous across the fracture, i.e., $\Delta p = p(+L_0/2) - p(-L_0/2) = 0$, because the fracture aperture (L_0) is small compared to the wavelength of the tube waves.[12,21,23] Eq. (13) with the continuation of pressure ($\Delta p = 0$) is equivalent to the linear-slip boundary condition,[47] which is a classical boundary condition for a solid–solid interface to describe elastic wave propagation across a thin layer, e.g., crack and fracture.[27,46] The linear-slip boundary condition is a special case of a nonwelded interface boundary condition,[48,49] where both stress and displacement are discontinuous.

The reflection and transmission problem at a nonwelded interface has extensively been studied in elastic wave propagation at fractures.[47,50,51] In Appendix B, we derive the tube-wave reflection and transmission coefficients at a fracture (Eqs. B1 and B2) represented by a nonwelded interface.

C. Representation of total tube wavefield using Green's functions

1. Representation theorem including nonwelded interfaces

In order to handle correctly the multiple scattering due to nonwelded interfaces, we use the representation theorem of general dynamic wave equation including nonwelded interfaces.[36] Coupling the representation theorem with our tube wave problem, we obtain the representation theorem of one-dimensional tube wavefield. Note that, due to the unified form of the reciprocity theorem,[38] our derivation can be easily extended to the scattering problems in two and three dimension in, e.g., acoustic, elastic or electromagnetic media. In this vein, the representation theorem is exploited in order to derive the two- and three-dimensional elastic scattering problems due to nonwelded interfaces.[40]

The representation theorem relates wavefields of two different states in which the medium parameters and boundary conditions can be different.[36] Here, we consider a true medium

response for one of the states and a reference medium response for the other state. By considering our tube-wave problem (Eqs. 2, 3 and 13), the representation theorem of tube wavefield can be expressed as,

$$
\begin{aligned}
&\bar{G}^{pq}(z',z'',\omega) - G^{pq}(z',z'',\omega) \\
&= \left[\bar{G}^{pq}(z',z_b,\omega)G^{vq}(z_b,z'',\omega) + \bar{G}^{pf}(z',z_b,\omega)G^{pq}(z_b,z'',\omega)\right] \\
&- \left[\bar{G}^{pq}(z',z_0,\omega)G^{vq}(z_0,z'',\omega) + \bar{G}^{pf}(z',z_0,\omega)G^{pq}(z_0,z'',\omega)\right] \\
&-i\omega\int_{z_0}^{z_b}\left[\bar{G}^{pq}(z',z,\omega)\Delta K_{\text{eff}}^{-1}(z)G^{pq}(z,z'',\omega) + \bar{G}^{pf}(z',z,\omega)\Delta\rho_f(z)G^{vq}(z,z'',\omega)\right]dz \\
&-i\omega\sum_{i=1}^{N}\eta^{(i)}\bar{G}^{pq}(z',z_i,\omega)G^{pq}(z_i,z'',\omega),
\end{aligned}
\tag{15}
$$

where we used the source-receiver reciprocity,[36] and $G^{ij}(z',z'',\omega)$ is the Green's function at z' of the acoustic pressure ($i=p$) or the vertical particle velocity ($i=v$) due to a point injection rate source ($j=q$) or a vertical force source ($j=f$) located at z''. G^{ij} and $\bar{G}^{ij}$ are, respectively, the Green's functions in the actual medium (K_{eff} and ρ_f) including the fracture (nonwelded interface characterized by η) and the Green's functions in the reference medium ($\bar{K}_{\text{eff}}$ and $\bar{\rho_f}$) without any fracture (without any nonwelded interface). $\Delta K_{\text{eff}}^{-1}$ and $\Delta\rho_f$ contain the differences in the medium parameters:

$$\Delta K_{\text{eff}}^{-1}(z) = K_{\text{eff}}^{-1}(z) - \bar{K}_{\text{eff}}^{-1}(z), \tag{16}$$

$$\Delta\rho_f(z) = \rho_f(z) - \bar{\rho}_f(z). \tag{17}$$

We consider N fractures which are located at z_i ($i=1,2,\cdots,N$) and characterized by the interface compliance $\eta^{(i)}$. The depth z', z'' and z_i are assumed to be located between the top of the borehole z_0 and the bottom of the borehole z_b (z-axis points downward, see Fig. 1):

$$z_0 < z_l < z_b, \tag{18}$$

where z_l is z', z'' or z_i.

At this point, we can choose any medium parameter for the reference Green's function $\bar{G}^{ij}$. Eq. (15) indicates that the scattered tube waves (difference between actual and reference Green's functions) are generated due to the presence of nonwelded interfaces (fourth term on the right-hand side of Eq. 15) as well as the contrasting medium parameters, i.e., $\Delta K_{\text{eff}}^{-1}$ and $\Delta\rho_f$ (third term on the right-hand side of Eq. 15). Because we would like to focus on the tube-wave scattering (reflection and transmission) due to the hydraulic fractures, we proceed

to consider a special case of Eq. (15) where the reference Green's function $\bar{G}^{ij}$ is derived from the actual medium parameters but without any fractures, i.e., $\Delta K_{\text{eff}}^{-1} = \Delta\rho_f = 0$. In this case, Eq. (15) is simplified as,

$$G^{pq}(z', z'', \omega) - \bar{G}^{pq}(z', z'', \omega) = \int_{z_0}^{z_b} \phi_s(z) \bar{G}^{pq}(z', z, \omega) G^{pq}(z, z'', \omega) dz, \tag{19}$$

$$\phi_s(z) = i\omega \sum_{i=1}^{N} \eta^{(i)} \delta(z - z_i), \tag{20}$$

where we call the function ϕ_s as *tube-wave scattering potential*. Note that, in order to derive Eq. (19), we also assumed that the medium parameters in the region outside of the integral path ($z \leq z_0$ and $z \geq z_b$) are homogenous in both the reference and the actual Green's functions. In this case, the Green's functions at the top (z_0) and the bottom (z_b) of the borehole contain only upgoing wave and downgoing wave, respectively. This condition cancels the contribution from the finite integral path in the representation theorem (first and second terms on the right-hand side of Eq. 15), which corresponds to an infinitely long borehole. Different and more realistic boundary conditions for the top and bottom of the borehole are considered in the numerical modeling section (Section V).

Note that Eq. (19) is useful in order to consider controlled tube-wave measurements using a logging tool.[12,17,52] An equation similar to Eq. (19) is used in Ref. 53 in order to remove the scattered waves due to borehole irregularities, modeled as a mass-balance boundary condition[41,54] which implicitly considers the nonwelded interface boundary condition.

2. Representation of tube-wave generation and scattering due to multiple fractures

In this subsection, we derive the equation for total tube wavefield which considers simultaneous effects of tube-wave generation and scattering (reflection and transmission) at multiple fractures. To this end, we consider the following procedure: (1) an incident plane P wave causes a pressure field in the borehole (p_{inc}), (2) the P wave generates tube waves at the intersection of the hydraulic fracture with an amplitude which is determined by the tube-wave generation amplitude ratio γ_g (Eq. 10), (3) the generated tube waves excite the Green's function G^{pq} which propagates along the borehole and generates scattered waves (reflection and transmission) at multiple fractures, and (4) the total tube wavefield is expressed as a

superposition of the tube wavefield generated at multiple fractures. We, therefore, define the total pressure field (p) as,

$$p(z) = \int_{z_0}^{z_b} \phi_g(z') G^{pq}(z, z') p_{\mathrm{inc}}(z') dz' + p_{\mathrm{inc}}(z), \tag{21}$$

where, ϕ_g is *tube-wave generation potential*:

$$\phi_g(z) = \sum_{i=1}^{N} \frac{2}{\rho_f c_T} \gamma_g^{(i)} \delta(z - z_i). \tag{22}$$

Note that the factor $2/\rho_f c_T$ is required due to the definition of Green's function (Eq. C1).

Using Eq. (21), the representation theorem (Eq. 19) becomes:

$$\begin{aligned} & p(z) - p_{\mathrm{inc}}(z) \\ & = \int_{z_0}^{z_b} \phi_g(z') \bar{G}^{pq}(z, z', \omega) p_{\mathrm{inc}}(z') dz' + \int_{z_0}^{z_b} \phi_s(z') \bar{G}^{pq}(z, z', \omega) \left[p(z') - p_{\mathrm{inc}}(z') \right] dz', \end{aligned} \tag{23}$$

where we used the source-receiver reciprocity,[36] and we changed the notation of z' to z and z'' to z', respectively. Eq. (23) is the main equation derived in this study. This equation indicates that the pressure field (p) including tube-wave generation and tube-wave scattering at multiple fractures is represented by the incident pressure field (p_{inc}), the reference Green's function ($\bar{G}^{pq}$), and the potential functions (ϕ_s and ϕ_g). Note that we exclude the scattering due to the contrasting medium parameters ($\Delta K_{\mathrm{eff}}^{-1} = \Delta \rho_f = 0$) to derive Eq. (23). Therefore, the right-hand side of Eq. (23) can be represented by the summation of the potential functions at descrete positions of the fractures (see Eq. 20 and Eq. 22). When one considers the scattering due to the contrasting medium parameters (nonzero $\Delta K_{\mathrm{eff}}^{-1}$ and $\Delta \rho_f$), then the integral for the contrasting medium parameters (third term on the right-hand side of Eq. 15) remains in the equation of the total tube wavefield, which is useful in numerically modeling tube waves in complex structures.

III. SCATTERING IMMEDIATELY AFTER GENERATION

In this section, we apply the equation of the total tube wavefield (Eq. 23) to a single fracture and show that it results in a new physical interpretation of the effective tube-wave generation amplitude in which the generation and scattering are mutually connected.

We consider that a single fracture is located at $z = z_1$ in a homogeneous medium characterized by tube-wave velocity c_T. In this case, the potential functions are written as

$\phi_g(z) = (2/\rho_f c_T)\gamma_g \delta(z - z_1)$ and $\phi_s(z) = i\omega\eta\delta(z - z_1)$, respectively. Assuming that we observe the pressure field at $z = z_2$, the total tube wavefield (Eq. 23) becomes,

$$p(z_2) - p_{\rm inc}(z_2) = \frac{2\gamma_g}{\rho_f c_T}\bar{G}^{pq}(z_2, z_1)p_{\rm inc}(z_1) + i\omega\eta\bar{G}^{pq}(z_2, z_1)\left[p(z_1) - p_{\rm inc}(z_1)\right]. \tag{24}$$

In order to obtain a relationship between the pressure field and the Green's function at coincident points, we consider the special case of $z_2 = z_1$ where the receiver is located just at the fracture. In this case, Eq. (24) can be rewritten as,

$$p(z_1) - p_{\rm inc}(z_1) = \frac{\gamma_g p_{\rm inc}(z_1)}{1 - i\omega\eta\bar{G}_0}\frac{2}{\rho_f c_T}\bar{G}_0, \tag{25}$$

where $\bar{G}_0$ is the Green's function at coincident points defined as,

$$\begin{aligned}\bar{G}_0 &\equiv \bar{G}^{pq}(z_1, z_1)\\ &= \frac{\rho_f c_T}{2},\end{aligned} \tag{26}$$

where we use Eq. (C1). Using Eq. (25), Eq. (24) becomes,

$$p(z_2) - p_{\rm inc}(z_2) = \frac{\gamma_g p_{\rm inc}(z_1)}{1 - i\omega\eta\bar{G}_0}\frac{2}{\rho_f c_T}\bar{G}^{pq}(z_2, z_1). \tag{27}$$

Eq. (27) shows that the pressure field due to the fracture ($p - p_{\rm inc}$) recorded at the receiver position (z_2) is represented by the generated amplitude $\gamma_g p_{\rm inc}$ multiplied by the factor $1/\left(1 - i\omega\eta\bar{G}_0\right)$ and the phase delay due to the propagation from z_1 to z_2, i.e., $2/\rho_f c_T \times \bar{G}^{pq}(z_2, z_1)$. This demonstrates that the generated tube waves are connected with the nonwelded interface with the interface compliance (η) immediately after generation. Eq. (27) implies that the interaction is *nonlinear* in terms of the interface compliance (η), which can be seen by expanding the amplitude factor of Eq. (27) as,

$$\begin{aligned}\frac{\gamma_g p_{\rm inc}}{1 - i\omega\eta\bar{G}_0} &= u_1/\left(1 - u_2\bar{G}_0\right)\\ &= u_1 + u_1\bar{G}_0u_2 + u_1\bar{G}_0u_2\bar{G}_0u_2 + u_1\bar{G}_0u_2\bar{G}_0u_2\bar{G}_0u_2 + \cdots,\end{aligned} \tag{28}$$

where,

$$\begin{aligned}u_1 &= \gamma_g p_{\rm inc},\\ u_2 &= i\omega\eta.\end{aligned} \tag{29}$$

Eq. (28) indicates that the interaction with the nonwelded interface is represented by an infinite series of the interface compliance (η) and the Green's function at coincident points

(G_0), which follows the discussion found in the classical wave theory.[55,56] From Eq. (28) one can see that the generated amplitude ($\gamma_g p_{\rm inc}$) determined from the boundary condition of Beydoun *et al.*[25] is equivalent to the zeroth order Born approximation in terms of the interface compliance (η). Note that Eq. (28) shows a slightly different form compared to the *nonlinear scattering* discussed in Ref. 55 (see equations 79 and 80 in Ref. 55), because we consider here nonwelded interface boundary condition and simultaneous effects of both generation and scattering at the coincident points.

We next derive the effective generation amplitude ratio. We interpret the first arriving event of tube wave traveling from the fracture (z_1) to the receiver position (z_2) as an effectively-generated tube wave. This implies that we consider the following equation:

$$p(z_2) - p_{\rm inc}(z_2) = \gamma_{\rm eff} p_{\rm inc}(z_1) \frac{2}{\rho_f c_T} \bar{G}^{pq}(z_2, z_1), \tag{30}$$

where $\gamma_{\rm eff}$ is the effective generation amplitude ratio which is evaluated at the receiver position. Comparing Eq. (27) and Eq. (30), we obtain,

$$\gamma_{\rm eff} = \frac{\gamma_g}{1 - i\omega\eta\bar{G}_0}. \tag{31}$$

This equation indicates that the effective generation amplitude ratio ($\gamma_{\rm eff}$) is represented by the interface compliance (η) as well as the generation amplitude ratio (γ_g) which is derived assuming that the generated tube wave does not perturb the pressure at the borehole (Beydoun's boundary condition, see Section II A). The generated tube wave at the fracture, however, indeed introduces pressure perturbation in the borehole and it introduces tube wave scattering with interface compliance (η), as discussed in Section II B and Eq. (28). This discussion and Eqs. (25), (30) and (31) reveal that the generated tube wave amplitude that we effectively evaluate at the receiver position contains two physical mechanisms: generation due to the fluid pulse injected from the fracture and the subsequent (nonlinear) scattering due to the pressure perturbation at the coinciding fracture, which we call the scattering immediately after generation (SIAG).

We show next that the effective generation amplitude (Eq. 31) with this new interpretation (SIAG) is consistent to the results obtained using a more realistic boundary condition (Bakku's original boundary condition, see Section II B and Appendix A 1). From Eq. (31) we obtain,

$$p_t^{\rm eff} = \frac{p_t}{1 - i\omega\eta\bar{G}_0}, \tag{32}$$

where p_t^{eff} is the effective generation amplitude evaluated at the receiver position. Substituting p_t (from Eq. 8), η (from Eq. 14), and $\bar{G}_0$ (from Eq. 26) in Eq. (32), we obtain,

$$p_t^{\text{eff}}(\omega) = \sigma_0 \frac{\omega}{k_r \alpha_f} \frac{c_T}{\alpha_{\text{eff}}} \frac{L_0}{R} \frac{\rho_f \alpha_{\text{eff}}^2}{L_0/Z} \times \left[\frac{iH_1(\zeta R)/H_0(\zeta R)}{1 + \frac{\omega}{k_r \alpha_f} \frac{c_T}{\alpha_{\text{eff}}} \frac{L_0}{R} iH_1(\zeta R)/H_0(\zeta R)} \right]. \tag{33}$$

This equation coincides with Eq. (A10) which is the result using the boundary condition that the pressure perturbation in the fracture at the borehole wall is equal to that in the borehole interior (Eqs. A5 and A6). This indicates that Bakku's boundary condition implicitly accounts for the simultaneous effect of tube-wave generation with Beydoun's boundary condition and SIAG. Note that Beydoun's boundary condition was considered in the foregoing studies[18,19,31] and Bakku's boundary condition was also considered earlier[26] without explicitly discussing the effect of SIAG.

IV. IMAGING MULTIPLE HYDRAULIC FRACTURES USING TOTAL TUBE WAVEFIELD

One important application of Eq. (23) is to obtain a new approach for imaging and characterizing hydraulic fractures using the total tube wavefield including generation and scattering (reflections and transmissions) due to the multiple fractures. In this vein, we present here a focusing analysis which is useful to resolve the position of the multiple fractures.

We define a focusing operator h (see Ref. 53) such that it satisfies:

$$\delta(z' - z'') = \int_{-\infty}^{\infty} h(z'', z) \bar{G}^{pq}(z', z) dz. \tag{34}$$

Applying this focusing operator to Eq. (23) results in,

$$\int_{-\infty}^{\infty} h(z'', z) p_{\text{scat}}(z) dz = \phi_g(z'') p_{\text{inc}}(z'') + \phi_s(z'') p_{\text{scat}}(z''), \tag{35}$$

where $p_{\text{scat}}(z) = p(z) - p_{\text{inc}}(z)$. Note that we assume here infinitely long borehole $-\infty \leq z \leq +\infty$. Eq. (35) indicates that the application of the focusing operator to the scattered tube wavefield (difference between the total and the incident pressure field) results in a temporal convolution of the pressure fields, tube-wave generation potential and scattering potential. Because these potentials have non-zero values only at the fractures (Eqs. 20 and 22), the right-hand side of Eq. (35) has non-zero values only at the fractures: this processing focuses the propagating tube waves to secondary source positions, which is useful to image

the hydraulic fractures. Note that, in practice, the focusing operator (h) can be numerically obtained from known values of the reference Green's function $\bar{G}^{pq}$.[53]

V. NUMERICAL EXAMPLE

In this section, we use Eq. (23) in order to predict the total tube wavefield. The detailed forward-modeling procedure using matrix inverse with/without boundary conditions at the top and bottom of the borehole is shown in Appendix C. We first consider a simple two-fracture model with an infinite borehole, and we check the generated tube wave and the reflection coefficients. We then consider a more realistic situation where multiple fractures are randomly distributed in a finite borehole and apply the imaging method discussed in the previous section. As we discussed in Appendix C, we consider the situation where hydraulic fractures are located within a homogeneous medium (characterized by c_T) and the tube waves are generated and scattered only due to the fractures and not due to contrasting medium parameters (i.e., $\Delta K_{\text{eff}}^{-1} = \Delta\rho_f = 0$), which is a typical case for open fractures in crystalline rocks[20] and in laboratory experiments.[12]

A. Efficacy of modeled tube wavefield

We consider a 250 m-long, water-filled vertical borehole in a homogeneous, impermeable background medium (V_P =6000 m/s, V_S =3300 m/s, ρ =2700 kg/m^3), with the borehole radius (R) of 7.5 cm. In this case, the tube wave velocity c_T becomes 1446 m/s (Eq. 5). Two open fractures with 2 mm aperture are located at 75 m and 190 m depth (Fig. 2). Here we calculate the fracture compliances (Z) assuming a thin layer of water without asperities,[30,46,48,57] i.e., $Z = L_0/K_w$ where K_w is the bulk modulus of water.

We consider here an infinitely long borehole (Eq. 23) to calculate the total tube wavefield p using the potential functions and the incident P wave (see Appendix C 1). We discretize the vertical axis at 10 cm interval, and we assume that the receivers are located at every 1 m (Fig. 2). The first arriving event with the P-wave velocity in Fig. 2 is the incident P wave. The tube waves are generated at the fractures, and they are reflected and transmitted (including multiple reflections) to produce the later arriving events (Fig. 2). We verify the modeled tube wavefield by estimating the reflection coefficients (Fig. 3a) and the tube-wave

generation amplitude ratio (Fig. 3b), which are estimated by extracting signals indicated by the white lines in Fig. 2 and dividing them in the frequency domain. The theoretical reflection coefficients are calculated using Eq. (B4), which shows that the tube-wave reflections are correctly modeled. The two theoretical curves for the tube-wave generation amplitude ratio are shown in Fig. 3(b). The solid line in Fig. 3(b) indicates the theoretical curve with the generation amplitude (p_t) derived from a realistic boundary condition (Eq. A10, Bakku's boundary condition) and the dashed line the theoretical curve derived from Beydoun's boundary condition (Eq. 8). As we discussed in Section III, the estimated amplitude ratio is smaller than that derived from Beydoun's boundary condition due to the effect of scattering immediately after generation (SIAG), and the estimated values are consistent with the theory with a more realistic boundary condition (Bakku's boundary condition).

B. Imaging multiple fractures

We next consider randomly-distributed 15 fractures (Fig. 4a). This is calculated from a Gaussian distribution with an average depth of 125 m and a standard deviation of 50 m. The random apertures (see the plot at the bottom of Fig. 4a) have an average of 2 mm and a standard deviation of 0.5 mm. We calculate the total tube wavefield due to the fractures, i.e., $p(z) - p_{\mathrm{inc}}(z)$, as shown in Fig. 4(a). Here we also consider the boundary conditions at the top and bottom of the borehole in the equation of total tube wavefield (Eq. C8), where the top of the borehole is a traction-free boundary and the bottom of the borehole is a rigid boundary (see Appendix C 2 for detail). One can see that the total tube wavefield is more complicated than that for 2 fractures.

We apply the focusing operator h to the tube wavefield (Fig. 4b and c), i.e., evaluating the left-hand side of Eq. (35). Figs. 4(b) and (c) are obtained by bandpass filtering the left-hand side of Eq. (35). The results (Figs. 4b and c) show that the propagation of tube waves are suppressed and they are focused at secondary source positions, which is useful in identifying the position of the hydraulic fractures. Note that due to the boundaries at the top and bottom of the borehole, tube waves are also focused at these depths (Fig. 4b). The resulting signals at the fractures (Fig. 4c) are temporal convolution of the tube wavefield and the potential functions (right-hand side of Eq. 35). We calculate the energy of each traces in the result (Fig. 4d). Fig. 4(d) indicates that the large amplitudes are located at the fracture

depth corresponding to large fracture apertures and at the depth where multiple fractures are located between the receivers.

VI. CONCLUSIONS

We derive an equation to represent the total tube wavefield including scattering (reflection and transmission) and generation at multiple hydraulic fractures. Our formulation has a great flexibility and we can implement any existing model that accounts for tube-wave generation and scattering. In this study, we consider a recent model which includes simultaneous effects of fluid viscosity, dynamic fluid flow, and fracture compliance.

We identify that the generated tube waves interact with the nonwelded interface immediately after generation. This interaction is nonlinear in terms of the interface compliance. The generated amplitude obtained from Beydoun's classical boundary condition,[25] where the generated tube wave does not perturb the pressure in the borehole, gives a zeroth order Born approximation (in terms of the interface compliance) for the generated amplitude obtained from a more realistic boundary condition[23,26] where the perturbation due to the generated tube wave is equivalent to that in the borehole interior. This new physical mechanism, i.e., scattering immediately after generation (SIAG, Eq. 31), is highly general and applicable to other models. For example, we can consider the effect of SIAG for a poroelastic layer (instead of the parallel-wall open fracture considered in this study) using the theory developed by Ref. 19 for the model of tube-wave generation and Ref. 22 for the model of tube-wave scattering. Representation of a layer with a finite thickness as a nonwelded interface is possible by using a quasi-static approximation, which is often used in nondestructive material testing.[48,58] Furthermore, this representation enables us to consider inclined or dipping fractures, for which the effects of generation and scattering have earlier been studied separately.[19,22,25]

We also propose the application of this new equation for predicting the total tube wavefield and imaging multiple hydraulic fractures. The application of the focusing operator derived from the reference Green's function results in the spatial focusing of the tube waves into the secondary source positions. The imaging results illustrate the temporal convolution of tube-wave generation potential, scattering potential and total wavefield. This offers the possibility to estimate the fracture parameters through estimating the potential functions

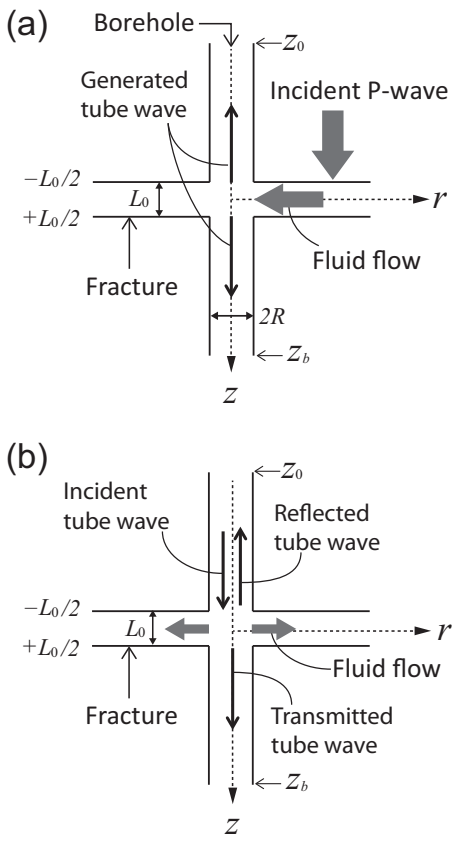

FIG. 1. (a) An incident plane P wave generates tube waves due to the fluid flow into a borehole. (b) The tube wave is reflected and transmitted due to the fluid flow into a fracture.

from the imaging results.

We anticipate that extending the formulation presented in this article to the scattering and generation of low-frequency guided waves in other fields of research (e.g., pipes immersed in a fluid or bones embedded in soft tissues) in terms of the scattering and generation potentials (Eqs. 20 and 22) will enable one to directly apply the theory to nondestructive material testing and medical sciences, where detecting and characterizing small defects/cracks/fractures along a cylindrical inclusion is important.

ACKNOWLEDGMENTS

We thank two anonymous reviewers for their helpfull reviews and comments that improved the manuscript. This work is supported by The Netherlands Research Centre for Integrated Solid Earth Science (ISES).

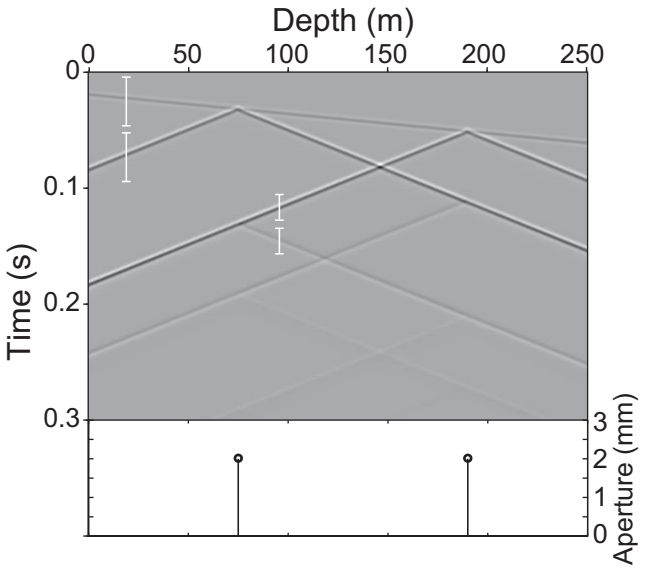

FIG. 2. Numerically modeled total tube wavefield (p) along a 250-m long fluid-filled borehole with two open fractures. The plot at the bottom shows the aperture distribution of the fractures. The white lines indicate the windows that are used to evaluate the tube-wave generation amplitude ratio and the reflection coefficients in Fig. 3.

Appendix A: Open fracture model including the effect of fracture compliance

1. Tube-wave generation amplitude

Bakku *et al.*[23] derived the tube-wave generation amplitude and the tube-wave transmission coefficient (tube-wave scattering) due to a horizontal, parallel-wall open fracture. Apart from other foregoing studies, Bakku *et al.*[23] considered the simultaneous effects of fluid viscosity, dynamic fluid flow (dynamic permeability), and fracture compliance. In this subsection, we briefly explain their theory. This is necessary in order to derive the generated amplitude using Beydoun's boundary conditions (Appendix A 2) which are suitable for investigating the simultaneous effects of tube-wave generation and scattering.

The dynamic fracture aperture (L) oscillates around the static aperture (L_0) due to the stress field with the fracture compliance (Z):

$$L(t) = L_0 + Z\left[p_F(t) - \sigma_n(t)\right], \tag{A1}$$

where p_F is the fluid-pressure perturbation in the fracture due to the closure of the fracture wall and σ_n is the external normal stress applied to the fracture wall, $\sigma_n(t) = \sigma_0 e^{-i\omega t}$.

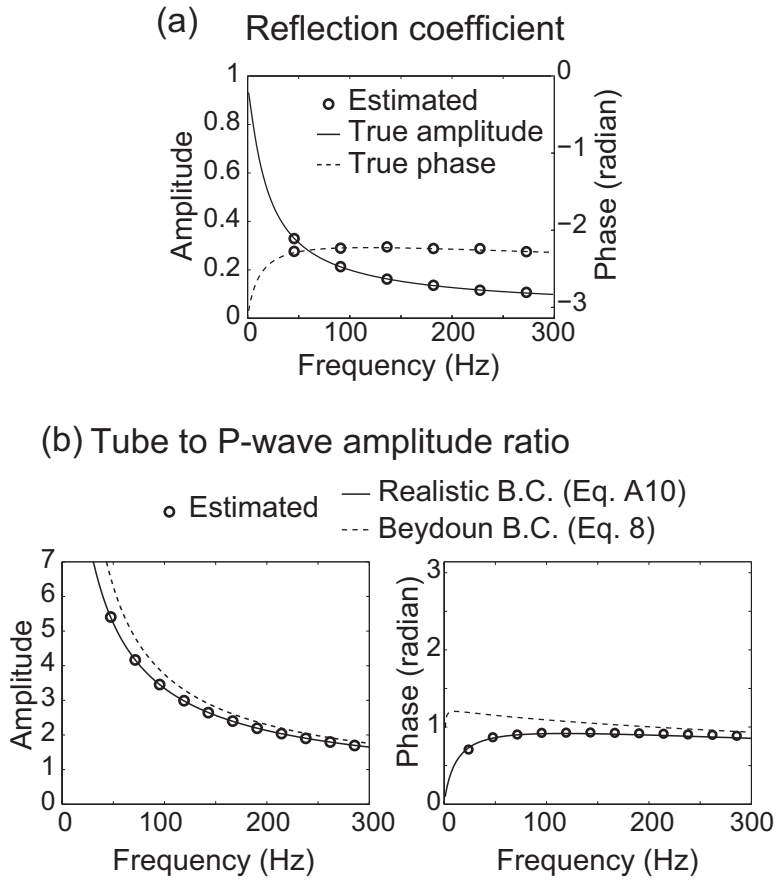

FIG. 3. (a) Estimated and theoretical reflection coefficients of the fracture. The estimated values are obtained from the modeled tube wave at 96 m depth (see the white lines in Fig. 2). (b) Estimated and theoretical tube-wave generation amplitude ratio of the fracture. The estimated values are obtained from the modeled tube wave at 20 m depth (see white lines in Fig. 2). The two theoretical curves are shown: Bakku's original theory including SIAG (solid lines) and Bakku's formulation solved using Beydoun's boundary condition, i.e., without considering SIAG (dashed lines).

Here, we consider the fracture compliance Z to be real positive valued.[23,29,46] Note that the dynamic fracture aperture (Eq. A1) is obtained assuming the incident stress to be uniform everywhere along the fracture.[18,23] There are alternative expressions for the dynamic fracture aperture: for example, Refs. 19, 25, and 26 assume the fracture aperture to be uniform everywhere along the fracture. Contrary to the foregoing models,[19,26] our model[18,23] has an additional term in the dynamic fracture aperture, which contains the dynamic fluid pressure and introduces separately the effect of the fracture compliance.

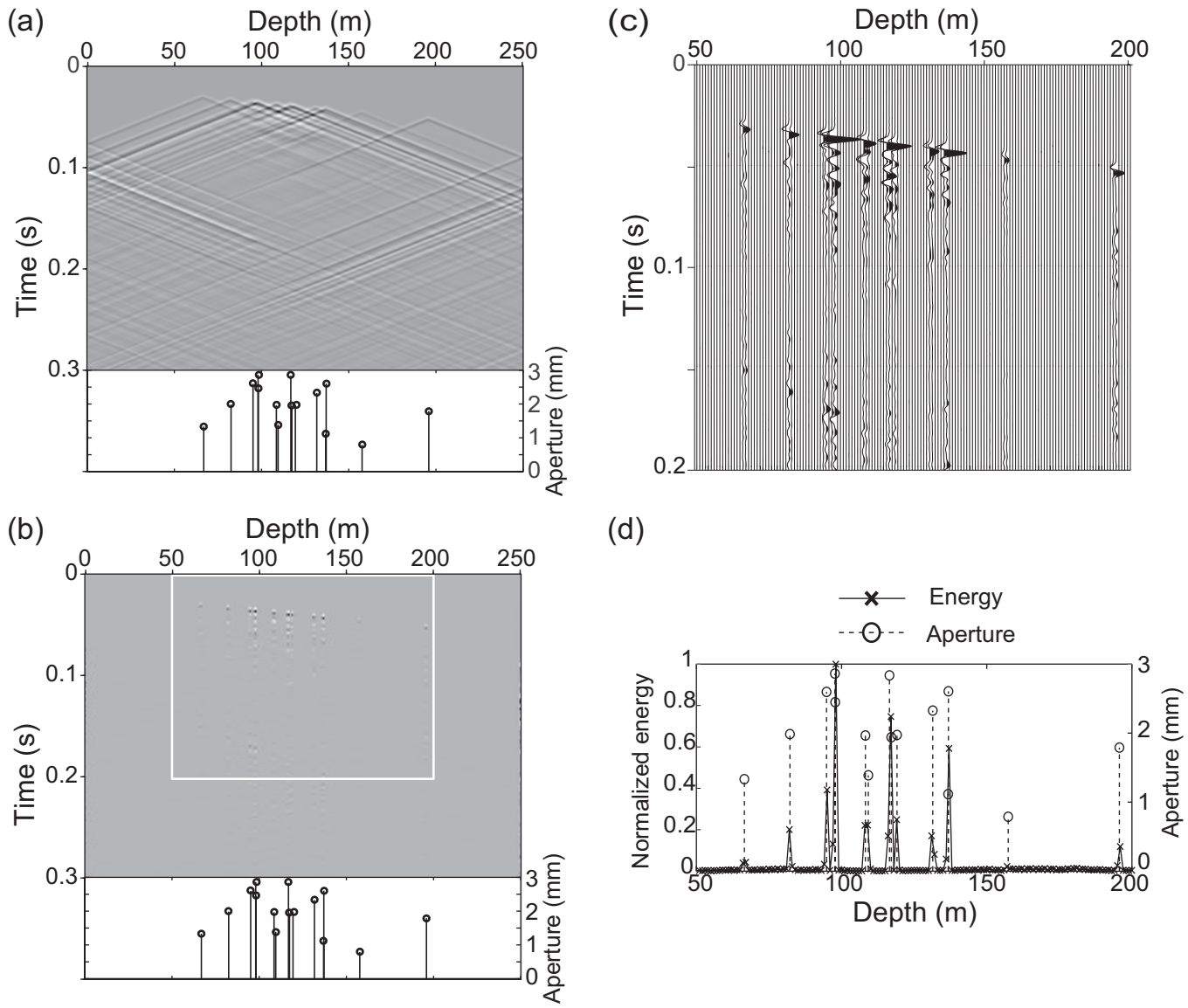

FIG. 4. (a) Numerically modeled, total tube wavefield due to fractures ($p - p_{\rm inc}$), with randomly-distributed 15 fractures. The plot at the bottom shows the aperture distribution of the fractures. (b) The result of the application of the focusing operator (h) to (a). (c) The wave signals in the white box shown in (b). (d) The normalized energy of each traces in (c) and the aperture distribution of the fractures.

By considering the mass conservation in the fracture assuming the axial symmetry of the problem, Bakku *et al.*[23] derived the following equation for the fluid-pressure field in the fracture (p_F):

$$\frac{\partial^2 p_F(r,\omega)}{\partial r^2} + \frac{1}{r}\frac{\partial p_F(r,\omega)}{\partial r} + \zeta^2 p_F(r,\omega) = \sigma_0 \frac{\rho_f Z \zeta^2 \alpha_{\rm eff}^2}{L_0}, \tag{A2}$$

where ζ is the effective radial wavenumber and α_{eff} is the effective fluid velocity in the fracture which are defined as,

$$\zeta = \frac{k_r \alpha_f}{\alpha_{\text{eff}}},$$
$$\alpha_{\text{eff}}^{-2} = \alpha_f^{-2} + \rho_f Z / L_0. \tag{A3}$$

Here, k_r is the radial wavenumber in the rigid fracture obtained by numerically solving the dispersion relation developed in Ref. 24 (see equations 14, 15 and 21 in Ref. 24). Note that k_r is a function of the kinematic fluid viscosity (ν), fluid velocity (α_f), static fracture aperture (L_0), and angular frequency (ω).

Note that Bakku *et al.*[23] derived Eq. (A2) assuming that the dynamic fluid flux (q_f) can be represented by that of a viscous fluid in an infinitely long, rigid (zero compliance) fracture:[24]

$$q_f(r,\omega) = -\frac{i\omega L_0}{k_r^2 \alpha_f^2 \rho_f} \frac{\partial p_F(r,\omega)}{\partial r}. \tag{A4}$$

The effect of the fracture compliance is then implemented in the part of the perturbation in the aperture (L) in the mass-conservation equation.[23]

Eq. (A2) is solved using the following boundary conditions:[23]

$$\left.\frac{\partial p_F(r,\omega)}{\partial r}\right|_{r=\infty} = 0, \tag{A5}$$
$$p_F(r,\omega)|_{r=R} = p_t. \tag{A6}$$

The first boundary condition states that the pressure is bounded at infinity and the second boundary condition indicates that the pressure perturbation in the fracture is equal to that in the borehole interior (i.e., generated tube-wave amplitude p_t) at the intersection ($r = R$). This boundary condition was considered in the foregoing study.[26] Finally, the pressure distribution (p_F) becomes,

$$p_F(r,\omega) = \left[p_t - \frac{\rho_f Z \alpha_{\text{eff}}^2}{L_0}\sigma_0\right] \frac{H_0(\zeta r)}{H_0(\zeta R)} + \frac{\rho_f Z \alpha_{\text{eff}}^2}{L_0}\sigma_0, \tag{A7}$$

where $H_n = H_n^{(1)}$ is a Hankel function of the first kind and order n. Note that the effective wavenumber ζ is obtained from the radial wavenumber k_r (Eq. A3). Following Ref. 23, we numerically obtain the fundamental mode solution for k_r, which has positive real and imaginary components for a positive ω. The example of the calculated ζ can be found in Ref. 23. Furthremore, the low- and high-frequency asymptotic solutions for k_r, and the

comparison between the dynamic fluid flow condition derived from k_r and that from the pore fluid flow theory[59] were extensively discussed in Ref. 60.

The amplitude of the generated tube wave (p_t) is defined as an equivalent volume source in the borehole (see Ref. 26 and references therein):

$$p_t(t) = \frac{\rho_f c_T}{2\pi R^2}\frac{dV}{dt}, \tag{A8}$$

$$\frac{dV}{dt} = -2\pi R q_f|_{r=R}\,. \tag{A9}$$

Therefore, we obtain,

$$p_t(\omega) = \sigma_0 \frac{\omega}{k_r \alpha_f}\frac{c_T}{\alpha_{\text{eff}}}\frac{L_0}{R}\frac{\rho_f \alpha_{\text{eff}}^2}{L_0/Z} \times \left[\frac{iH_1(\zeta R)/H_0(\zeta R)}{1+\frac{\omega}{k_r\alpha_f}\frac{c_T}{\alpha_{\text{eff}}}\frac{L_0}{R} iH_1(\zeta R)/H_0(\zeta R)}\right]. \tag{A10}$$

2. Tube-wave generation amplitude with Beydoun's boundary condition

In this subsection, we derive the alternative expression of pressure distribution (p_F) and generated amplitude (p_t) using boundary conditions that are different from those considered in the previous subsection. Beydoun *et al.*[25] assumed that the fluid pulse injected into the borehole does not significantly perturb the borehole pressure. It replaces the boundary condition of Eq. (A6) by,

$$p_F(r,\omega)|_{r=R} = 0. \tag{A11}$$

Note that Eq. (A11) appears differently than the equations in Appendix A in Ref. 25, because their definition of pressure p is the total pressure field (static pressure plus the perturbation) whereas the definition of pressure p_F in this paper considers only the perturbation in pressure.

Solving Eq. (A2) for the pressure field in the fracture using Beydoun's boundary conditions (Eqs. A5 and A11) gives,

$$p_F(r,\omega) = \frac{\rho_f Z \alpha_{\text{eff}}^2}{L_0}\sigma_0\left[1-\frac{H_0(\zeta r)}{H_0(\zeta R)}\right]. \tag{A12}$$

Following the same procedure to obtain the tube wave amplitude (p_t) gives (see previous subsection),

$$p_t(\omega) = \sigma_0 \frac{i\omega c_T}{k_r \alpha_f}\frac{\rho_f Z \alpha_{\text{eff}}}{R}\frac{H_1(\zeta R)}{H_0(\zeta R)}. \tag{A13}$$

3. Pressure distribution due to tube-wave scattering

We consider here that the traveling tube wave along the borehole propagates across the fracture (Fig. 1b). In this case, the pressure distribution p_F can be obtained using Eq. (A2) with the following boundary conditions:

$$\left.\frac{\partial p_F(r,\omega)}{\partial r}\right|_{r=\infty} = 0, \tag{A14}$$

$$p_F(r,\omega)|_{r=R} = p. \tag{A15}$$

The second equation indicates that the pressure in the fracture is equivalent to the borehole pressure at the intersection. Furthermore, here we do not consider the external source term present in Eqs. (A1) and (A2), i.e., $\sigma_0 = 0$. Therefore, we obtain,

$$p_F(r,\omega) = p\frac{H_0(\zeta r)}{H_0(\zeta R)}. \tag{A16}$$

Appendix B: Reflection and transmission coefficients at a nonwelded interface

Here we derive the reflection and transmission coefficients of tube waves interacting with the fracture, which is represented by a nonwelded interface (Eq. 13). The theoretical reflection and transmission coefficients at a nonwelded interface is widely available in elastic wave propagation literature.[47,50,51] For the scalar wave propagation across a nonwelded interface as discussed in Ref. 47, the reflection (R_C) and transmission (T_C) coefficients at the nonwelded interface within a homogeneous medium are written as,

$$R_C = \frac{i\omega\eta Z_T}{2 - i\omega\eta Z_T}, \tag{B1}$$

$$T_C = \frac{2}{2 - i\omega\eta Z_T}, \tag{B2}$$

$$Z_T = = \rho_f c_T. \tag{B3}$$

Note that we define the coefficients considering the acoustic pressure field. Substituting the expression of η (Eq. 14) in Eqs. (B1) and (B2) we obtain,

$$R_C = -\frac{\omega\zeta c_T k_r^{-2}\alpha_f^{-2} \times iL_0H_1(\zeta R)/RH_0(\zeta R)}{1 + \omega\zeta c_T k_r^{-2}\alpha_f^{-2} \times iL_0H_1(\zeta R)/RH_0(\zeta R)}, \tag{B4}$$

$$T_C = \frac{1}{1 + \omega\zeta c_T k_r^{-2}\alpha_f^{-2} \times iL_0H_1(\zeta R)/RH_0(\zeta R)}. \tag{B5}$$

These equations have the same form as equation (4a) and (4b) in Ref. 12. When we consider the rigid formation (rigid borehole and rigid fracture, i.e., $c_T = \alpha_f$ and $k_r = \zeta = \omega/\alpha_f$), we reproduce exactly the same results as Ref. 12.

Appendix C: Forward modeling

1. Infinite borehole

In this subsection, we show the application of the new equation (Eq. 23) to forward-model the total tube wavefield. We consider here an infinitely long borehole and in the next subsection a finite borehole with boundary conditions at the top and bottom of the borehole.

We consider that the reference Green's function ($\bar{G}^{pq}$) in Eq. (23) is derived considering a homogeneous medium without any fracture. From Eqs. (2) and (3), the Green's functions in the homogeneous medium read,

$$\bar{G}^{pq}(z, z_S, \omega) = \frac{\rho_f c_T}{2} e^{i\omega|z-z_S|c_T^{-1}}, \tag{C1}$$

$$\bar{G}^{vq}(z, z_S, \omega) = \frac{\mathrm{sgn}(z-z_S)}{2} e^{i\omega|z-z_S|c_T^{-1}}. \tag{C2}$$

We use Eq. (23) to solve unknown pressure field (p), which implies the assumption that the actual medium has the same medium parameters as the reference medium. This is the situation where the hydraulic fractures are located within the homogeneous medium (characterized by c_T) and the tube waves are generated and scattered only due to the fractures and not due to the contrasting medium parameters (i.e., $\Delta K_{\mathrm{eff}}^{-1} = \Delta\rho_f = 0$). In this vein, tube waves due to open fractures often dominate in crystalline rocks,[20] where there are no seismically-detectable geological layered structures. By using nonzero $\Delta K_{\mathrm{eff}}^{-1}$ and $\Delta\rho_f$, however, we can also model the total tube wavefield due to the contrasting medium parameters, as well as due to the fractures.

Our problem is to solve Eq. (23) for unknown pressure field (p) from the known values of incident pressure field (p_{inc}), reference Green's functions ($\bar{G}^{ij}$) and the potential functions (ϕ_g and ϕ_s). Here we numerically solve Eq. (23) by discretizing the integral path and then apply direct matrix inverse. We apply linear spatial discretization to the depth $z_0 \le z \le z_b$ such that the vector $\mathbf{p}$ contains $(p_0, p_1, \cdots, p_k, \cdots, p_M)^T$ where p_k indicates the total pressure at the kth spatial point, i.e., $p_k = p(z_0 + k\Delta z)$.

Eq. (23) can be written in the matrix-vector form as,

$$\mathbf{p} = \mathbf{p}_{\text{inc}} + \mathbf{M}\mathbf{p} + \mathbf{K}\mathbf{p}_{\text{inc}}, \tag{C3}$$

where,

$$\mathbf{M} = \begin{pmatrix} \phi_{s,0}\bar{G}^{pq}_{0,0}\Delta z & \phi_{s,1}\bar{G}^{pq}_{0,1}\Delta z & \cdots & \phi_{s,M}\bar{G}^{pq}_{0,M}\Delta z \\ \phi_{s,0}\bar{G}^{pq}_{1,0}\Delta z & \phi_{s,1}\bar{G}^{pq}_{1,1}\Delta z & \cdots & \phi_{s,M}\bar{G}^{pq}_{1,M}\Delta z \\ \vdots & \vdots & \ddots & \vdots \\ \phi_{s,0}\bar{G}^{pq}_{M,0}\Delta z & \phi_{s,1}\bar{G}^{pq}_{M,1}\Delta z & \cdots & \phi_{s,M}\bar{G}^{pq}_{M,M}\Delta z \end{pmatrix}, \tag{C4}$$

$$\mathbf{K} = \begin{pmatrix} \Delta\phi_0\bar{G}^{pq}_{0,0}\Delta z & \Delta\phi_1\bar{G}^{pq}_{0,1}\Delta z & \cdots & \Delta\phi_M\bar{G}^{pq}_{0,M}\Delta z \\ \Delta\phi_0\bar{G}^{pq}_{1,0}\Delta z & \Delta\phi_1\bar{G}^{pq}_{1,1}\Delta z & \cdots & \Delta\phi_M\bar{G}^{pq}_{1,M}\Delta z \\ \vdots & \vdots & \ddots & \vdots \\ \Delta\phi_0\bar{G}^{pq}_{M,0}\Delta z & \Delta\phi_1\bar{G}^{pq}_{M,1}\Delta z & \cdots & \Delta\phi_M\bar{G}^{pq}_{M,M}\Delta z \end{pmatrix}, \tag{C5}$$

$$\Delta\phi_k = \phi_{g,k} - \phi_{s,k}, \tag{C6}$$

where $\phi_{g,k}$ and $\phi_{s,k}$ are, respectively, the tube-wave generation potential and scattering potential at kth spatial point, and $G^{pq}_{k,l}$ is the pressure Green's function due to the source at lth spatial point and the receiver at kth point, i.e., $\bar{G}^{pq}(z_0 + k\Delta z, z_0 + l\Delta z, \omega)$.

Eq. (C3) can be solved using the direct matrix inverse in order to obtain the unknown pressure field $\mathbf{p}$ as,

$$\mathbf{p} = (\mathbf{I} - \mathbf{M})^{-1}(\mathbf{I} + \mathbf{K})\,\mathbf{p}_{\text{inc}}, \tag{C7}$$

where $\mathbf{I}$ is the identity matrix. We use MATLAB's LU decomposition scheme to evaluate Eq. (C7).

2. Finite borehole

We consider here that tube waves which are generated due to incident P wave are reflected at the top and bottom of the borehole. To this end, we assume that actual Green's functions satisfy the boundary condition that the top of the borehole is the traction-free boundary $G^{pq}(z_0, z) = 0$, and the bottom of the borehole is the rigid boundary $G^{vq}(z_b, z) = 0$. The rest of the assumptions are same as in the previous subsection. Note that one may alternatively think of the effect of the stiffness of the formation in the bottom of the borehole, which was considered in Ref. 61.

Using the boundary conditions described above, Eq. (23) can be written as,

$$
\begin{aligned}
& p(z) - p_{\mathrm{inc}}(z) \\
& = \bar{G}^{vq}(z_b, z)\left[p(z_b) - p_{\mathrm{inc}}(z_b)\right] + \bar{G}^{pq}(z, z_0)\left[v_z(z_0) - v_z^{\mathrm{inc}}(z_0)\right] \\
& + \int_{z_0}^{z_b} \phi_g(z')\bar{G}^{pq}(z, z', \omega) p_{\mathrm{inc}}(z') dz' + \int_{z_0}^{z_b} \phi_s(z')\bar{G}^{pq}(z, z', \omega)\left[p(z') - p_{\mathrm{inc}}(z')\right] dz', \quad \text{(C8)}
\end{aligned}
$$

where we used the source-receiver reciprocity,[36] and v_z^{inc} is the vertical particle velocity due to the incident pressure (p_{inc}). The first and second terms on the right-hand side of Eq. (C8) is the contribution due to the finite integral path and the boundary conditions at the top and bottom of the borehole.

As in the previous subsection, we write Eq. (C8) in the matrix-vector form (Eq. C3). To this end, we consider the following approximation:

$$
v_z(z_0) - v_z^{\mathrm{inc}}(z_0) \approx (i\omega\rho_f \Delta z)^{-1} p(z_0 + \Delta z) - \left[(i\omega\rho_f \Delta z)^{-1} + (\rho_f V_P)^{-1}\right] p_{\mathrm{inc}}(z_0). \quad \text{(C9)}
$$

This approximation is derived from the equation of motion (Eq. 3), the forward difference of $p(z)$ at $z = z_0$, the boundary condition of the pressure field $p(z_0) - p_{\mathrm{inc}}(z_0) = 0$, and the relation between the incident pressure field and the velocity field (see Ref. 9), i.e., $v_z^{\mathrm{inc}}(z_0) = (\rho_f V_P)^{-1} p_{\mathrm{inc}}(z_0)$.

Using Eq. (C9), the equation of the total tube wavefield (Eq. C8) can be written in the

matrix-vector form as Eq. (C3), but with the matrices defined as,

$$\mathbf{M} = \begin{pmatrix} \phi_{s,0}\bar{G}^{pq}_{0,0}\Delta z & \phi_{s,1}\bar{G}^{pq}_{0,1} + \bar{G}^{pq}_{0,0}A & \phi_{s,2}\bar{G}^{pq}_{0,2}\Delta z & \cdots & \phi_{s,M-1}\bar{G}^{pq}_{0,M-1}\Delta z & \phi_{s,M}\bar{G}^{pq}_{0,M}\Delta z + \bar{G}^{vq}_{M,0} \\ \phi_{s,0}\bar{G}^{pq}_{1,0}\Delta z & \phi_{s,1}\bar{G}^{pq}_{1,1} + \bar{G}^{pq}_{1,0}A & \phi_{s,2}\bar{G}^{pq}_{1,2}\Delta z & \cdots & \phi_{s,M-1}\bar{G}^{pq}_{1,M-1}\Delta z & \phi_{s,M}\bar{G}^{pq}_{1,M}\Delta z + \bar{G}^{vq}_{M,1} \\ \vdots & \vdots & \vdots & \ddots & \vdots & \vdots \\ \phi_{s,0}\bar{G}^{pq}_{M,0}\Delta z & \phi_{s,1}\bar{G}^{pq}_{M,1} + \bar{G}^{pq}_{M,0}A & \phi_{s,2}\bar{G}^{pq}_{M,2}\Delta z & \cdots & \phi_{s,M-1}\bar{G}^{pq}_{M,M-1}\Delta z & \phi_{s,M}\bar{G}^{pq}_{M,M}\Delta z + \bar{G}^{vq}_{M,M} \end{pmatrix}, \tag{C10}$$

$$\mathbf{K} = \begin{pmatrix} \Delta\phi_0\bar{G}^{pq}_{0,0}\Delta z - \bar{G}^{pq}_{0,0}B & \Delta\phi_1\bar{G}^{pq}_{0,1}\Delta z & \cdots & \Delta\phi_{M-1}\bar{G}^{pq}_{0,M-1}\Delta z & \Delta\phi_M\bar{G}^{pq}_{0,M}\Delta z - \bar{G}^{vq}_{M,0} \\ \Delta\phi_0\bar{G}^{pq}_{1,0}\Delta z - \bar{G}^{pq}_{1,0}B & \Delta\phi_1\bar{G}^{pq}_{1,1}\Delta z & \cdots & \Delta\phi_{M-1}\bar{G}^{pq}_{1,M-1}\Delta z & \Delta\phi_M\bar{G}^{pq}_{1,M}\Delta z - \bar{G}^{vq}_{M,1} \\ \vdots & \vdots & \ddots & \vdots & \vdots \\ \Delta\phi_0\bar{G}^{pq}_{M,0}\Delta z - \bar{G}^{pq}_{M,0}B & \Delta\phi_1\bar{G}^{pq}_{M,1}\Delta z & \cdots & \Delta\phi_{M-1}\bar{G}^{pq}_{M,M-1}\Delta z & \Delta\phi_M\bar{G}^{pq}_{M,M}\Delta z - \bar{G}^{vq}_{M,M} \end{pmatrix}, \tag{C11}$$

$$A = (i\omega\rho_f\Delta z)^{-1}, \tag{C12}$$

$$B = (i\omega\rho_f\Delta z)^{-1} + (\rho_f V_P)^{-1}. \tag{C13}$$

The velocity Green's function at the coincident points at the bottom of the borehole ($\bar{G}^{vq}_{M,M}$) is defined as,

$$\begin{aligned} \bar{G}^{vq}_{M,M} &= \lim_{z\to z_b^-} \bar{G}^{vq}(z_b, z, \omega) \\ &= \frac{1}{2}, \end{aligned} \tag{C14}$$

where we use Eq. (C2).

REFERENCES

[1]D. Chimenti and A. H. Nayfeh, J. Appl. Phys. **58**, 4531 (1985).

[2]P. B. Nagy and L. Adler, J. Appl. Phys. **66**, 4658 (1989), doi:10.1063/1.343822.

[3]Z. Su, L. Ye, and Y. Lu, J. Sound. Vib. **295**, 753 (2006), doi:10.1016/j.jsv.2006.01.020.

[4]M. Talmant and G. Quentin, J. Appl. Phys. **63**, 1857 (1988).

[5]J. Cheeke, X. Li, and Z. Wang, J. Acoust. Soc. Am. **104**, 3678 (1998).

[6]V. C. Protopappas, D. I. Fotiadis, and K. N. Malizos, Ultrasound. Med. Biol. **32**, 693 (2006), doi:10.1016/j.ultrasmedbio.2006.02.001.

[7]P. Moilanen, IEEE. T. Ultrason. FERR. **55**, 1277 (2008), doi:10.1109/TUFFC.2008.790.

[8]M. Biot, J. Appl. Phys. **23**, 997 (1952), doi:10.1063/1.1702365.

[9]M. Schoenberg, Geophysics **51**, 1191 (1986).

[10]M. Lowe, D. Alleyne, and P. Cawley, Ultrasonics **36**, 147 (1998), doi:10.1016/S0041-624X(97)00038-3.

[11]A. Croxford, P. Wilcox, B. Drinkwater, and G. Konstantinidis, P. Roy. Soc. Lond. A. Mat. **463**, 2961 (2007), doi:10.1098/rspa.2007.0048.

[12]B. Hornby, D. Johnson, K. Winkler, and R. Plumb, Geophysics **54**, 1274 (1989), doi:10.1190/1.1442587.

[13]R. Mindlin and H. McNiven, J. Appl. Mech. **27**, 145 (1960), doi:10.1115/1.3643889.

[14]C. H. Cheng and M. N. Toksöz, Geophysics **46**, 1042 (1981), doi:10.1190/1.1441242.

[15]A. Aydin, Mar. Petrol. Geol. **17**, 797 (2000), doi:10.1016/S0264-8172(00)00020-9.

[16]C. A. Wibberley and T. Shimamoto, J. Struct. Geol. **25**, 59 (2003), doi:10.1016/S0191-8141(02)00014-7.

[17]F. L. Paillet and J. E. White, Geophysics **47**, 1215 (1982), doi:10.1190/1.1441384.

[18]E. Hardin, C. Cheng, F. Paillet, and J. Mendelson, J. Geophys. Res. **92**, 7989 (1987), doi:10.1029/JB092iB08p07989.

[19]Y. Li, W. Rabbel, and R. Wang, Geophys. J. Int. **116**, 739 (1994), doi:10.1111/j.1365-246X.1994.tb03294.x.

[20]T. Kiguchi, H. Ito, Y. Kuwahara, and T. Miyazaki, Isl. Arc. **10**, 348 (2001), doi:10.1111/j.1440-1738.2001.00333.x.

[21]F. Mathieu, *Application of full waveform acoustic logging data to the estimation of reservoir permeability*, M.S. thesis, Massachusetts Institute of Technology (1984).

[22]X. M. Tang and C. Cheng, Geophys. Prosp. **41**, 165 (1993), doi:10.1111/j.1365-2478.1993.tb00864.x.

[23]S. K. Bakku, M. Fehler, and D. Burns, Geophysics **78**, D249 (2013), doi:10.1190/geo2012-0521.1.

[24]X. Tang and C. Cheng, J. Geophys. Res. **94**, 7567 (1989), doi:10.1029/JB094iB06p07567.

[25]W. Beydoun, C. Cheng, and M. Toksöz, J. Geophys. Res. **90**, 4557 (1985), doi:10.1029/JB090iB06p04557.

[26]A. M. Ionov, Geophys. Prosp. **55**, 71 (2007), doi:10.1111/j.1365-2478.2006.00577.x.

[27]L. Pyrak-Nolte, L. Myer, and N. Cook, J. Geophys. Res. **95**, 8617 (1990),

doi:10.1029/JB095iB06p08617.

[28]L. Pyrak-Nolte and J. Morris, Int. J. Rock. Mech. Min. **37**, 245 (2000), doi:10.1016/S1365-1609(99)00104-5.

[29]R. Lubbe, J. Sothcott, M. Worthington, and C. McCann, Geophys. Prosp. **56**, 239 (2008), doi:10.1111/j.1365-2478.2007.00688.x.

[30]S. Minato and R. Ghose, Geophys. J. Int. **206**, 56 (2016), doi:10.1093/gji/ggw138.

[31]R. D. Cicerone and M. N. Toksöz, J. Geophys. Res. **100**, 4131 (1995), doi:10.1029/94JB02982.

[32]H. Moses, Phys. Rev. **102**, 559 (1956), doi:10.1103/PhysRev.102.559.

[33]R. G. Newton, Geophys. J. Int. **65**, 191 (1981), doi: 10.1111/j.1365-246X.1981.tb02708.x.

[34]C.-W. Nan and F.-S. Jin, Phys. Rev. B. **48**, 8578 (1993), doi:10.1103/PhysRevB.48.8578.

[35]A. B. Weglein, F. A. Gasparotto, P. M. Carvalho, and R. H. Stolt, Geophysics **62**, 1975 (1997), doi: 10.1190/1.1444298.

[36]K. Wapenaar, Geophysics **72**, SM5 (2007), doi:10.1190/1.2750646.

[37]E. Larose, A. Derode, M. Campillo, and M. Fink, J. Appl. Phys. **95**, 8393 (2004), doi:10.1063/1.1739529.

[38]K. Wapenaar, E. Slob, and R. Snieder, Phys. Rev. Lett. **97**, 234301 (2006), doi:10.1103/PhysRevLett.97.234301.

[39]I. Vasconcelos, R. Snieder, and H. Douma, Phys. Rev. E. **80**, 036605 (2009), doi:10.1103/PhysRevE.80.036605.

[40]S. Minato and R. Ghose, Geophysics **80**, A25 (2015), doi:10.1190/geo2014-0406.1.

[41]J. E. White, *Underground sound: Application of seismic waves*, Vol. 253 (Elsevier Amsterdam, 1983).

[42]S. K. Chang, H. L. Liu, and D. L. Johnson, Geophysics **53**, 519 (1988), doi:10.1190/1.1442483.

[43]L. Pyrak-Nolte and D. Nolte, Geophys. Res. Lett **19**, 325 (1992), doi:10.1029/91GL03179.

[44]S. Biwa, S. Hiraiwa, and E. Matsumoto, Ultrasonics **47**, 123 (2007), doi:10.1016/j.ultras.2007.08.005.

[45]A. Baird, J. Kendall, and D. Angus, Geophysics **78**, WA111 (2013), doi:10.1190/geo2012-0288.1.

[46]P. Nagy, J. Nondestruct. Eval. **11**, 127 (1992), doi:10.1007/BF00566404.

[47]M. Schoenberg, J. Acoust. Soc. Am. **68**, 1516 (1980), doi:10.1121/1.385077.

[48]S. I. Rokhlin and Y. J. Wang, J. Acoust. Soc. Am. **89**, 503 (1991), doi:10.1121/1.400374.

[49]K. Wapenaar, E. Slob, and J. Fokkema, J. Geophys. Res. **109**, B10301 (2004), doi:10.1029/2004JB003002.

[50]B. Gu, R. Suárez-Rivera, K. T. Nihei, and L. R. Myer, J. Geophys. Res. **101**, 25337 (1996), doi:10.1029/96JB01755.

[51]S. Chaisri and E. S. Krebes, J. Geophys. Res. **105**, 28045 (2000), doi:10.1029/2000JB900296.

[52]R. T. Coates, Geophys. Prosp. **46**, 153 (1998), doi:10.1046/j.1365-2478.1998.00079.x.

[53]G. C. Herman, P. A. Milligan, Q. Dong, and J. W. Rector, Geophysics **65**, 745 (2000), doi:10.1190/1.1444773.

[54]K. Tezuka, C. H. A. Cheng, and X. M. Tang, Geophysics **62**, 1047 (1997), doi:10.1190/1.1444206.

[55]M. C. W. van Rossum and T. M. Nieuwenhuizen, Rev. Mod. Phys. **71**, 313 (1999), doi:10.1103/RevModPhys.71.313.

[56]K. Wapenaar, E. Slob, and R. Snieder, Geophysics **75**, SA27 (2010), doi:10.1190/1.337435.

[57]E. Liu, J. Hudson, and T. Pointer, J. Geophys. Res. **105**, 2981 (2000).

[58]J.-M. Baik and R. B. Thompson, J. Nondestruct. Eval. **4**, 177 (1984).

[59]D. L. Johnson, J. Koplik, and R. Dashen, J. Fluid. Mech. **176**, 379 (1987), doi:10.1017/S0022112087000727.

[60]X. Tang, C. Cheng, and M. N. Toksöz, J. Acoust. Soc. Am. **90**, 1632 (1991), doi:10.1121/1.401904.

[61]A. M. Ionov and G. A. Maximov, Geophys. J. Int. **124**, 888 (1996), doi:10.1111/j.1365-246X.1996.tb05643.x.

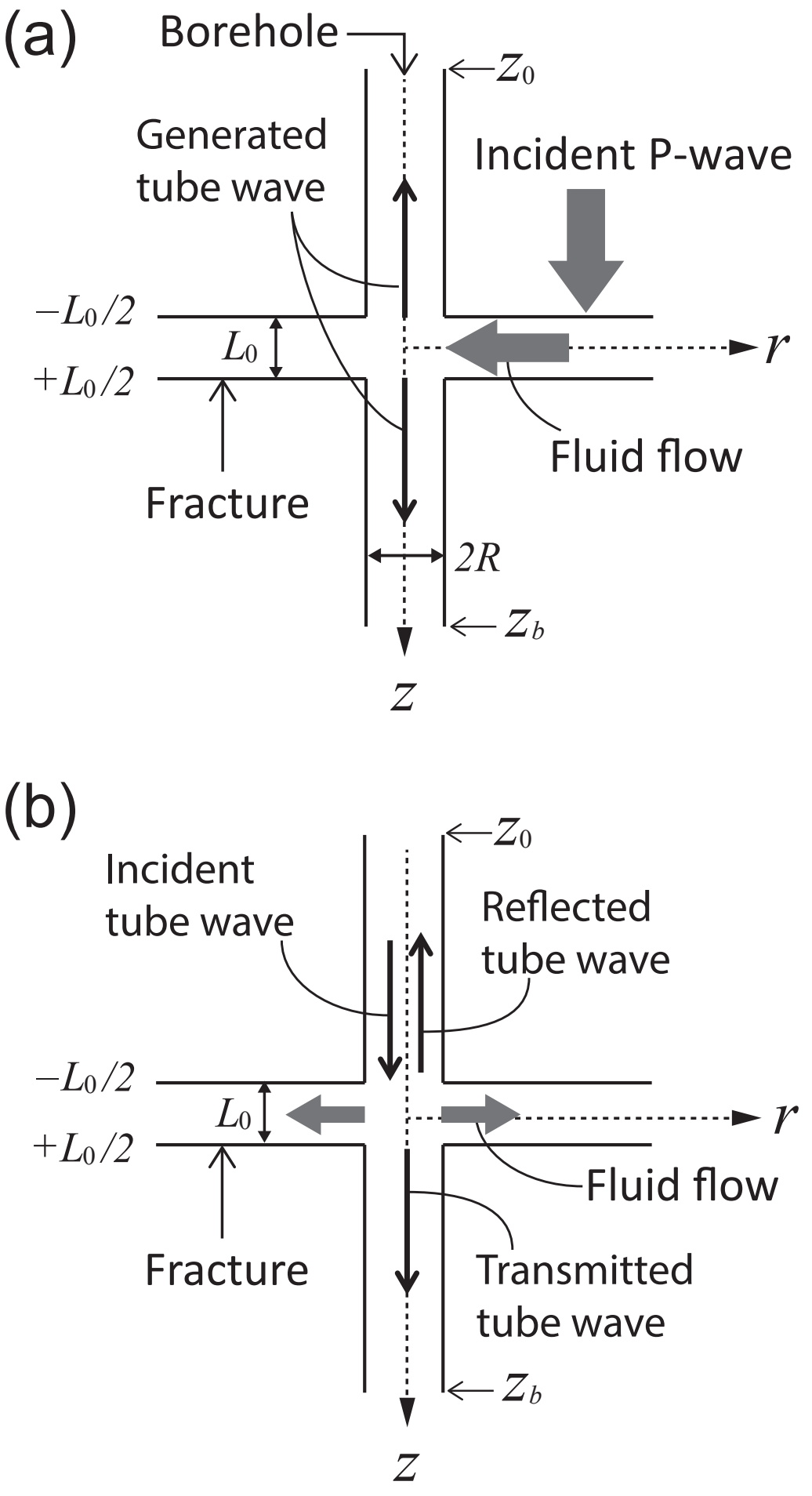
(a)
Borehole
z_0
Generated
tube wave
Incident P-wave
$-L_0/2$
L_0
$+L_0/2$
r
Fluid flow
Fracture
$2R$
z_b
z
(b)
z_0
Incident
tube wave
Reflected
tube wave
$-L_0/2$
L_0
$+L_0/2$
r
Fluid flow
Fracture
Transmitted
tube wave
z_b
z

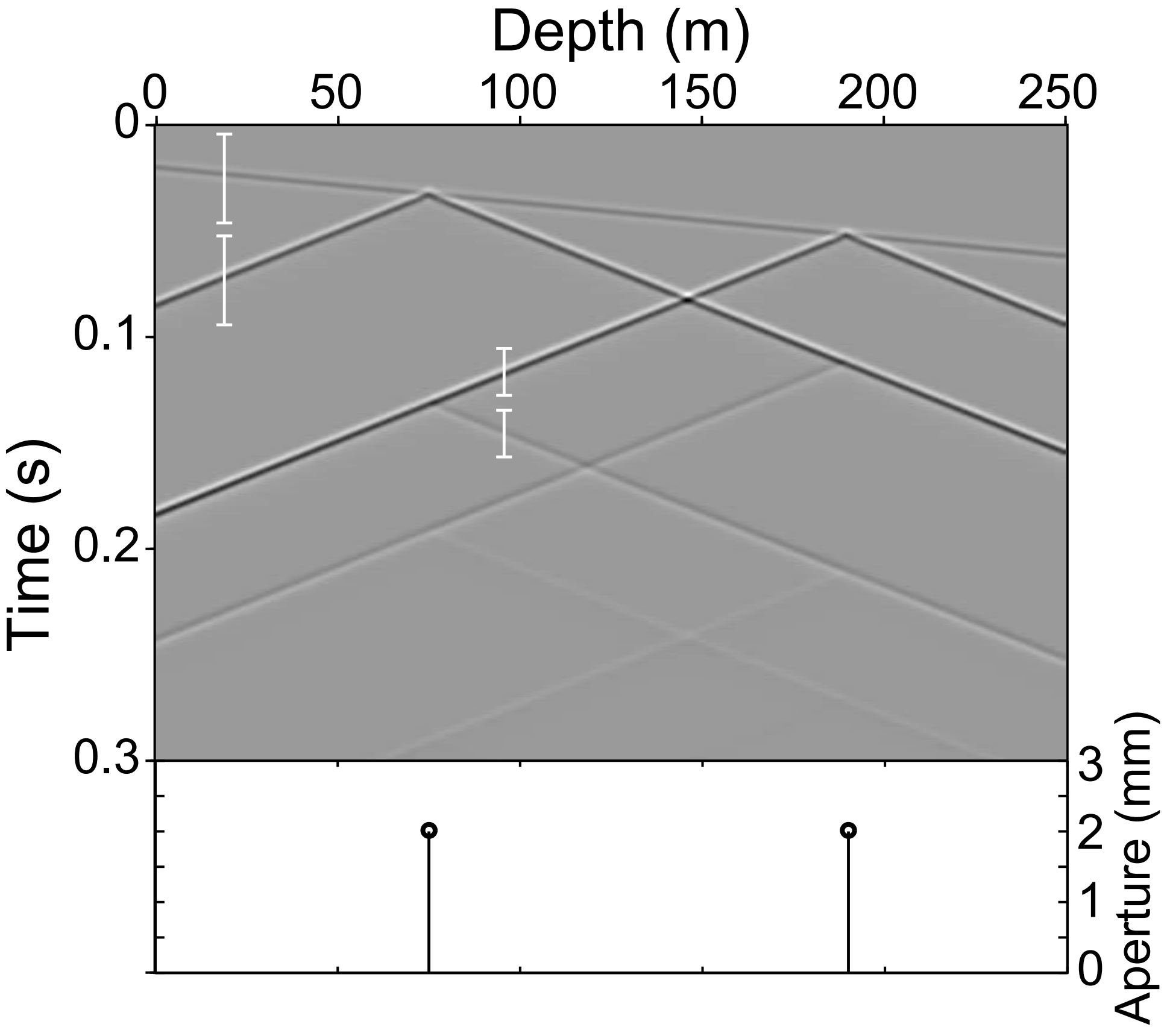
Depth (m)
0
50
100
150
200
250
Time (s)
0
0.1
0.2
0.3
Aperture (mm)
0
1
2
3

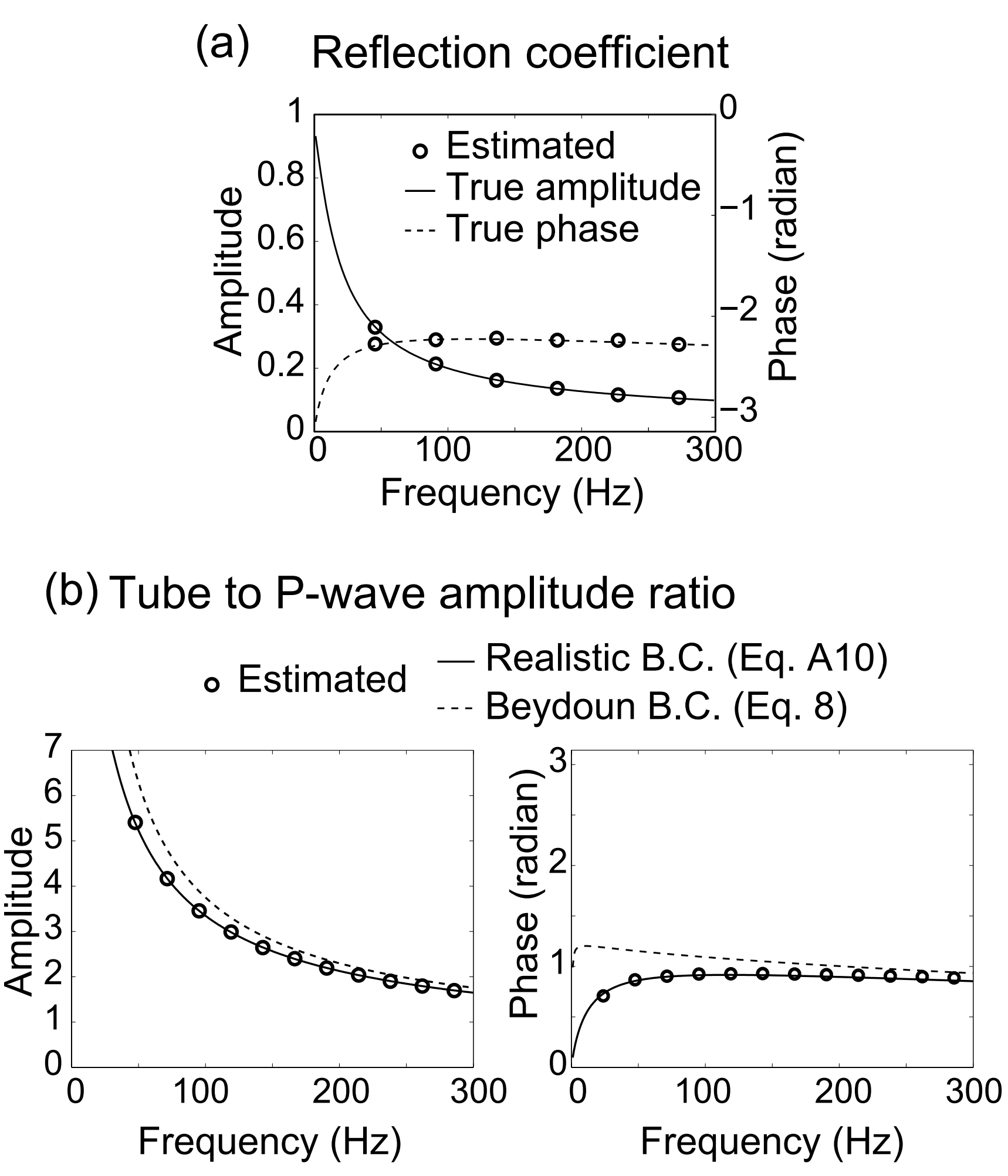
(a) Reflection coefficient
Estimated
True amplitude
True phase
Amplitude
Phase (radian)
Frequency (Hz)
(b) Tube to P-wave amplitude ratio
Estimated
Realistic B.C. (Eq. A10)
Beydoun B.C. (Eq. 8)
Amplitude
Phase (radian)
Frequency (Hz)
Frequency (Hz)

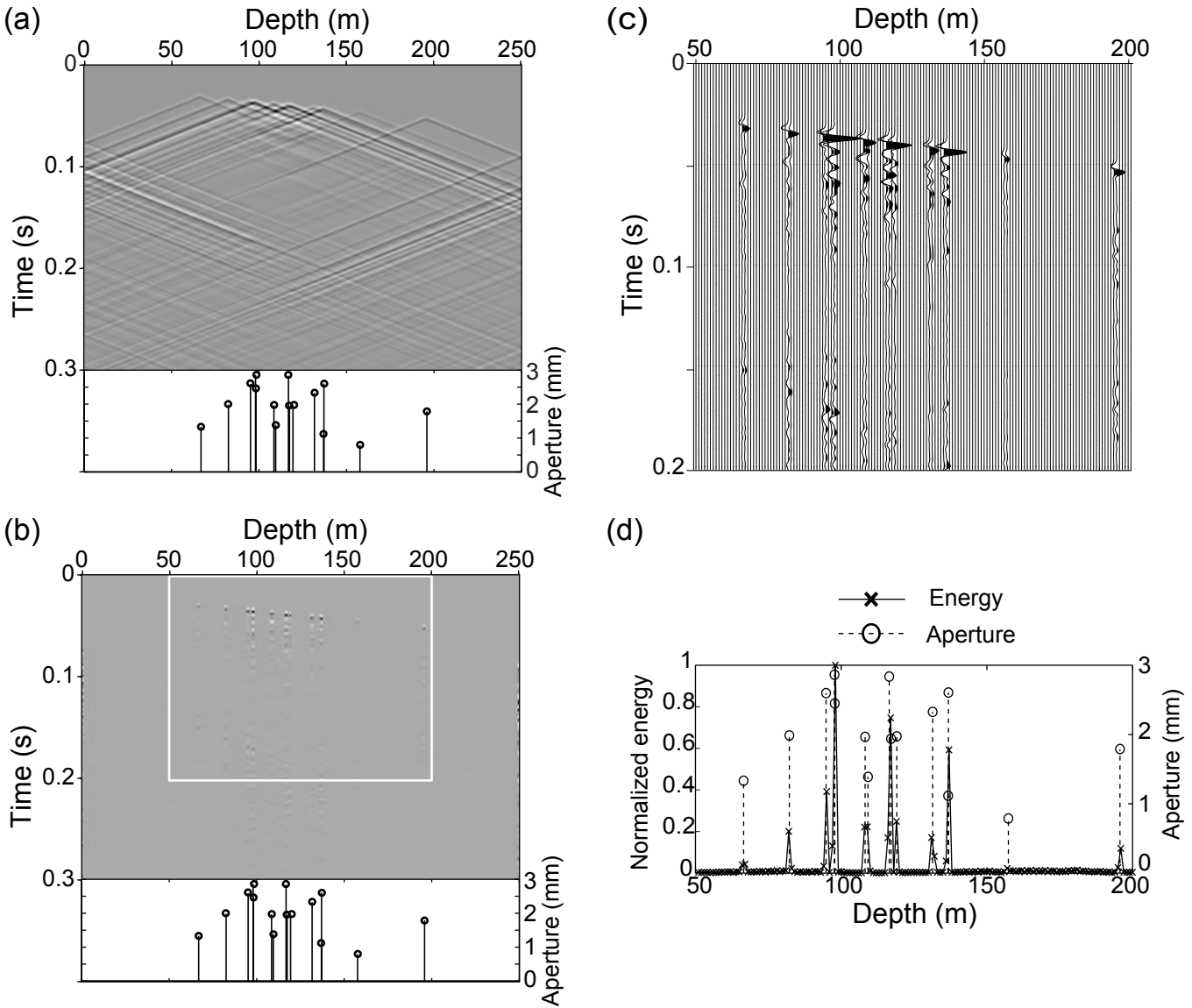
(a)
Depth (m)
0
50
100
150
200
250
Time (s)
0
0.1
0.2
0.3
Aperture (mm)
0
1
2
3
(b)
Depth (m)
Time (s)
Aperture (mm)
(c)
Depth (m)
50
100
150
200
Time (s)
0
0.1
0.2
(d)
Energy
Aperture
Normalized energy
0
0.2
0.4
0.6
0.8
1
Aperture (mm)
Depth (m)